



Systemic Sympathoexcitation Was Associated with Paraventricular Hypothalamic Phosphorylation of Synaptic CaMKII α and MAPK/ErK

Olalekan M. Ogundele^{1*}, Fernando A. Rosa², Rohan Dharmakumar³, Charles C. Lee¹ and Joseph Francis^{1*}

¹ Department of Comparative Biomedical Sciences, Louisiana State University School of Veterinary Medicine, Baton Rouge, LA, United States, ² Departamento de Clínica, Cirurgia e Reprodução Animal, Faculdade de Medicina Veterinária, Universidade Estadual Paulista, Araçatuba, Brazil, ³ Department of Biomedical Sciences, Cedars-Sinai Medical Center Biomedical Imaging Research Institute, Los Angeles, CA, United States

OPEN ACCESS

Edited by:

Yulong Li,
University of Nebraska Medical
Center, United States

Reviewed by:

Qing-Hui Chen,
Michigan Technological University,
United States
Ali Nasimi,
Isfahan University of Medical
Sciences, Iran

*Correspondence:

Olalekan M. Ogundele
ogundele@lsu.edu
Joseph Francis
jfrancis@lsu.edu

Specialty section:

This article was submitted to
Autonomic Neuroscience,
a section of the journal
Frontiers in Neuroscience

Received: 06 March 2017

Accepted: 21 July 2017

Published: 03 August 2017

Citation:

Ogundele OM, Rosa FA,
Dharmakumar R, Lee CC and
Francis J (2017) Systemic
Sympathoexcitation Was Associated
with Paraventricular Hypothalamic
Phosphorylation of Synaptic CaMKII α
and MAPK/ErK.
Front. Neurosci. 11:447.
doi: 10.3389/fnins.2017.00447

Systemic administration of adrenergic agonist (Isoproterenol; ISOP) is known to facilitate cardiovascular changes associated with heart failure through an upregulation of cardiac toll-like receptor 4 (TLR4). Furthermore, previous studies have shown that cardiac tissue-specific deletion of TLR4 protects the heart against such damage. Since the autonomic regulation of systemic cardiovascular function originates from pre-autonomic sympathetic centers in the brain, it is unclear how a systemically driven sympathetic change may affect the pre-autonomic paraventricular hypothalamic nuclei (PVN) TLR4 expression. Here, we examined how change in PVN TLR4 was associated with alterations in the neurochemical cytoarchitecture of the PVN in systemic adrenergic activation. After 48 h of intraperitoneal 150 mg/kg ISOP treatment, there was a change in PVN CaMKII α and MAPK/ErK expression, and an increase in TLR4 expression. This was seen as an increase in p-MAPK/ErK, and a decrease in synaptic CaMKII α expression in the PVN ($p < 0.01$) of ISOP treated mice. Furthermore, there was an upregulation of vesicular glutamate transporter (VGLUT 2; $p < 0.01$) and a decreased expression of GABA in the PVN of Isoproterenol (ISOP) treated WT mice ($p < 0.01$). However, after a PVN-specific knockdown of TLR4, the effect of systemic administration of ISOP was attenuated, as indicated by a decrease in p-MAPK/ErK ($p < 0.01$) and upregulation of CaMKII α ($p < 0.05$). Additionally, loss of inhibitory function was averted while VGLUT2 expression decreased when compared with the ISOP treated wild type mice and the control. Taken together, the outcome of this study showed that systemic adrenergic activation may alter the expression, and phosphorylation of preautonomic MAPK/ErK and CaMKII α downstream of TLR4. As such, by outlining the roles of these kinases in synaptic function, we have identified the significance of neural TLR4 in the progression, and attenuation of synaptic changes in the pre-autonomic sympathetic centers.

Keywords: β_2 R, MAPK/ErK, CaMKII α , TLR4, VGLUT2, GABA, sympathoexcitation

INTRODUCTION

Paraventricular hypothalamic adrenergic neurotransmission forms part of the pre-autonomic control of systemic cardiovascular function (Xu et al., 2012; Lee et al., 2013; Patel et al., 2016). Furthermore, abnormalities in the expression of β -adrenergic receptors (β AR) or its hyperactivation in cardiac tissue have been described in rodent models of heart failure (Madamanchi, 2007; Giudice et al., 2016; Yamazaki et al., 2016).

The neural control of systemic cardiovascular function is mediated through multiple feedback loops involving the preautonomic sympathetic centers of the brain and peripheral mechanoreceptor systems. As such, an increase in the activity of the PVN, or brain stem projections to the intermediolateral gray column may increase heart rate. Evidently, an increase in sympathetic activation promotes the release of norepinephrine, which activates cardiac β -adrenergic receptors.

β ARs are G-protein coupled receptors expressed on the surface of neurons, cardiac cells, hepatocytes, endothelial cells and adrenal glands (Ichikawa et al., 2016; Romberger et al., 2016). In the presence of a β AR agonist, such as isoproterenol (ISOP), G-protein is released leading to the activation of PIP_3 which initiate cascades of signaling events involving the phosphorylation of downstream kinases (Dawaliby et al., 2016; Ranjan et al., 2016). In support of this proposition, the transcription of *Ras/Raf/MAPK* genes increases after ISOP treatment and is associated with TLR4 signaling (Kim et al., 2006; Lu et al., 2014; Theccanat et al., 2016). In addition, the expression of TLR4 in cardiac tissue may determine the efficacy of β AR agonists as (such as ISOP) agents to induce heart failure. As such, a cardiac tissue-specific deletion of TLR4 prevents cardiac tissue damage after ISOP treatment (Kim et al., 2006).

The relative abundance of β ARs on various cell types in the nervous and vascular system makes it (that is β ARs) a suitable target for disease models and therapeutic targeting (Badshah et al., 2016; Ranjan et al., 2016). Furthermore, activation of *Ras/Raf*-downstream of β ARs-suggests the involvement of pro-inflammatory receptors and associated pathways in systemic cardiovascular changes (Cho et al., 2016). Although previous studies have described changes in systemic inflammatory response in heart failure models, how a systemic driven change may affect the neurochemical architecture of the preautonomic centers is yet to be elucidated.

Previous studies have shown that β AR signaling promotes inflammation and sympathoexcitation simultaneously (Mo et al., 2014; Morioka et al., 2014). Through its effect on TLR4 and NMDAR, β AR affects nNOS, and GABA neurotransmission in the brain; further increasing excitatory glutamatergic potentials (Sharma et al., 2011; Lethbridge et al., 2012; Di Mauro et al., 2013). Similarly, TLR4-mediated MAPK/ErK activation leads to inflammation via phosphorylation of calcium-calmodulin dependent kinase II alpha (CaMKII α) (Mizukami et al., 2015; Yu et al., 2016). Thus, we hypothesize that attenuating MAPK/ErK inflammatory signaling events, in the PVN neurons, may reduce the severity

of sympathoexcitation by reducing the phosphorylation of CaMKII α .

Despite the available evidence on the role of TLR4 in β ARA-mediated tissue damage, the significance of neural (PVN) TLR4 during systemic β ARA remains unknown. In this study, we sought to evaluate the effect of systemically driven β AR activation on the neurochemical cytoarchitecture of the PVN. Specifically, the study highlights the significance of PVN TLR4 in altering synaptic kinases, excitatory, and inhibitory neurotransmitter balance after systemic β AR activation.

METHODS

WT and Transgenic Mice Strains

Adult C57BL/6 (WT; $n = 20$) and transgenic C57BL/TLR4^{loxp/loxp} ($n = 20$) were procured from the Jackson Laboratory, United States. C57BL (VGAT)-Venus mice ($n = 10$), previously characterized by Wang et al. (2009), were obtained from Dr. Janice Nagle at Wesleyan University. All animals used for this experiment weighed between 22 and 25 g. Animals were kept under standard laboratory condition and handled using NIH guidelines for animal care and use in research. All protocols used were reviewed and approved by the Institutional Animal Care and Use Committee of the Louisiana State University.

Anatomical Tract Tracing

The projections from the PVN were identified using fluorescent retrograde anatomical tract tracing and immunohistochemistry. Flame pulled glass pipettes were back-filled with mineral oil and mounted on a Nanoject (Drummond Instruments). The tip of the pipette was trimmed with forceps to increase the width to 200 μ m and reduce resistance to the injected bolus. Rhodamine B + Amine [10,000 MW] (*Life Technologies*; Molecular Probe) was diluted (10%) in saline and drawn into tip of the glass pipette. The coordinate of the Nucleus of solitary tract (NTS) was determined using a stereotaxic apparatus (NTS: Anteroposterior -6.96 mm, Mediolateral $+1.35$ mm; Franklin and Paxinos, 1997). A dental drill was used to remove the bone on the marked AP/ML intersection until the dura became visible. The exposed brain area was kept moist with oxygenated artificial cerebrospinal fluid [aCSF; in mM 125 NaCl, 25 NaHCO₃, 3 KCl, 1.25 NaH₂PO₄, 1 MgCl₂, 2 CaCl₂, and 25 Glucose] throughout the duration of the experiment. The pipette (Nanoject) was lowered gradually into the NTS (Dorsoventral: $+5.5$ mm) following which two boli (5 nL each) were injected at 120 s interval. After a resting period of 3 min, the pipette was lowered further (DV: $+6.0$ mm) to label the SolL/SolV area. After a 7-day survival period, animals were euthanized following which the whole brain was removed and kept in ice-cold oxygenated aCSF. Vibrotome sliced coronal slices (500 μ m thick) exposing the PVN (Bregma -0.58 mm to -1.22 mm) or NTS were fixed in 4% 10 mM phosphate buffered paraformaldehyde (4% PB PFA). In subsequent processing, 60 μ m thick cryostat sections were obtained from the fixed slices and labeled further in immunofluorescence methods.

Adenoviral Gene Expression and Tissue Specific PVN TLR4 Knockdown

AAV-CMV-eGFP and AAV-CMV-*Cre*-eGFP were procured from the University of Iowa Vector Core and stored at -80°C . TLR4^{loxP/loxP} mice were anesthetized using Ketamine/Xylazine (100mg/Kg;10mg/Kg body weight). The PVN was targeted stereotaxically for injections at coordinates relative to the bregma [AP -0.85 , ML $+1.5$ mm, DV $+5.5$ mm] (Franklin and Paxinos, 1997). Control (AAV-CMV-eGFP; $n = 10$ TLR4^{loxP/loxP} mice) or *Cre*-expressing AAV (AAV-CMV-*Cre*-eGFP; $n = 10$ TLR4^{loxP/loxP} mice) was injected into the PVN (500 nL) using a low resistance flame pulled glass pipette (200 μm wide; Lee et al., 2017). The pipette was filled with mineral oil and mounted on a Nanoject (Drummond Instruments, USA). After exposing the dura at the designated coordinates, adenoviral cocktail was aspirated into the tip of the pipette and checked for flow before being lowered into the neural tissue. The injections were done in multiple boli of 23 nL each at 60 s interval. After the last injection, the pipette stayed in position for 180 s before it was gradually withdrawn. AAV gene expression (eGFP reporter) was verified 3 weeks after the injection in wet mount brain slices; using an Olympus BX 51 Fluorescence microscope.

β AR Activation in WT and Transgenic Mice

Isoproterenol (Sigma, USA) was diluted in normal saline and administered in two separate intraperitoneal injections of 150 mg/kg (per injection) per animal (24 h' interval; Gupta et al., 2013). ISOP treatment was done in the following groups; WT/ISOP ($n = 10$), TLR4^{loxP/loxP}/ISOP ($n = 10$) and TLR4^{Cre/-}/ISOP ($n = 10$). The animals were euthanized 24 h after the last injection to obtain brain (PVN) sections for immunofluorescence. A separate group of $n = 10$ WT mice were treated with normal saline (i.p.).

Echocardiography

Cardiac function was measured using Toshiba Aplio echocardiographic machine as described previously (Dange et al., 2014).

Whole-Cell Patch-Clamping Electrophysiology

To assess physiological effects in the brains of some animals, after 48 h of ISOP acute treatment, animals were decapitated following which the whole brain was removed and kept in ice-cold oxygenated artificial cerebrospinal fluid (ACSF; in mM 125 NaCl, 25 NaHCO₃, 3 KCl, 1.25 NaH₂PO₄, 1 MgCl₂, 2 CaCl₂, and 25 Glucose). Vibratome sectioned coronal brain sections (400 μm thick) containing the PVN (Bregma -0.58 to -1.22 mm) were prepared in cold oxygenated artificial cerebrospinal fluid (ACSF) and transferred to oxygenated ACSF at 34°C for recovery (1 h). Subsequently, the brain slices were moved to a perfusion chamber mounted on an Olympus BX 51 phase contrast microscope. To record from neurons using the perforated patch technique, freshly aliquoted 3 mg of Amphotericin B was dissolved in 50 μl of dimethyl sulfoxide (DMSO) and stored at -20°C . Subsequently, 8 μl of Amphotericin B solution was added to 2 ml of intracellular pipette solution in mM

135 Potassium gluconate, 7 NaCl, 10 4-(2hydroxy ethyl)-1-piperazineethanesulfonic gluconate, 1-2Na₂ATP, 0.3 Guanosine Trisphosphate (GTP) and MgCl₂; the pH was adjusted with KOH and final Osmolality was set at 290 mOsm; Amphotericin B (0.24 mg/ml) following which it was kept on ice and stored away from light. Flame pulled glass pipette electrode (with resistance 3–5 M Ω) were prepared on a P-97 pipette puller (Stutter Instruments) and filled with the intracellular solution containing Amphotericin B. Using a micromanipulator, the electrode was visually guided to create a perforated patch (12–15 min) to isolate single-cell potentials (mV) in current clamp mode. Only cells with access resistance of 5–20 M Ω were recorded. Frequency (Hz) of evoked membrane depolarization potential was detected using Multiclamp 700B Amplifier and Digidata 1440A digital acquisition system (Molecular Instruments) after a step current was injected (60pA). Analysis of evoked action potentials was done in ClampFit (Axon Instrument, Sunnyvale, CA).

Western Blotting and Protein Quantification

For western blot analyses, 15 μl brain tissue lysate containing 15 μg of protein was processed for SDS-PAGE electrophoresis for $n = 7$ samples per group. After subsequent western blotting (wet transfer), Polyvinylidene fluoride membrane (PVDF) was incubated in Tris-buffered saline (with 0.01% Tween 20) (TBST) for 15 min in TBST at room temperature. Subsequently, the membrane was blocked in 3% Bovine serum albumin (prepared in TBST) for 50 min at room temperature. The protein of interest, and control (Homer-1 and GAPDH) were detected using the following primary antibodies; Mouse anti-CaMKII α (Cell Signaling-#50049), Rabbit anti p-CaMKII α (Cell Signaling-#12716S), Rabbit anti MAPK/ErK (Cell Signaling- #9102S), Rabbit anti p-MAPK/ErK (4370S), Rabbit anti NMDAR1 (abcam-# ab17345), Rabbit anti GABA_BR (abcam-#ab166604), Rabbit anti GAPDH (Cell Signaling-#517S), Rabbit anti Homer1 (Cell Signaling-#8231), Mouse anti TLR4 (abcam-# 76B357.1) and Rabbit anti NeuN-Alexa 488 Conjugate (abcam-#ab190195). All primary antibodies were diluted in the blocking solution at 1:1,000. Subsequently, the primary antibodies were detected using HRP-conjugated secondary antibodies (goat anti-rabbit-#65-6120 and goat anti-mouse-#65-6520; Invitrogen; dilution of 1:5,000 or 1:10,000) following which the reaction was developed using a chemiluminescence substrate (Thermo Fisher-#34579).

Cardiac Histology

Cardiac tissue was stained in Hematoxylin and Eosin ($n = 5$ per group) to demonstrate the general morphology of the ventricular wall using the methods of Fischer et al. (2008). Images were acquired in Nanozoomer (Hamatsu, USA). The affected area was determined in using Image J (NIH, USA).

Immunohistochemistry

WT and transgenic mice ($n = 10$ per group) were deeply anesthetized in isoflurane and perfused transcardially through the left ventricle using 10 mM phosphate buffered saline.

Subsequently, 4% phosphate buffered paraformaldehyde (PB-PFA) was introduced for perfusion fixation. The whole brain was harvested through cranial dissection and fixed in 4% PB-PFA overnight, following which it was transferred to 4% PB-PFA containing 30% Sucrose for cryopreservation. Free-floating cryostat sections (40 μm) were collected into 10 mM PBS stored away from light (4°C). Before the commencement of staining, the sections were washed 3 times (5 min each) in 10 mM PBS (pH 7.4). To block non-specific binding, sections were incubated in normal Goat serum (Vector Labs), prepared in 10 mM PBS (with 0.03% Triton-X 100), at room temperature for 1 h. Subsequently, the sections were washed 3 times in PBS and moved to a primary antibody solution for overnight incubation at 4°C. Primary antibodies [Mouse anti-CaMKII α (1:100; Cell Signaling-#50049), Guinea pig anti-VGLUT 2 (1:250; EMD Millipore-AB2251), Rabbit anti-GABA (1:200; Abcam-ab8891), Rabbit anti-MAPK/ErK1/ErK2 (1:100; Cell Signaling-#9102)] were prepared in 10 mM PBS, 0.03% Triton X-100 and Normal Goat Serum. In further processing, the sections were washed (as described previously) and incubated in secondary antibody solution [Goat anti-Rabbit Alexa-568, Goat anti-Guinea pig Alexa-568, and Goat anti-Mouse Alexa-568 (1:1,000), 10 mM PBS, 0.03% Triton X-100 and Normal Goat Serum] for 1 h at room temperature in a dark enclosure. Labeled sections were

washed and mounted on gelatin coated slides with plain anti-fade mounting medium (Vector Labs).

Confocal Microscopy and Cell Quantification

Imaging of adenoviral (AAV-CMV-eGFP or AAV-CMV-Cre-eGFP) gene reporter expression (*eGFP*) was performed on serial cryostat coronal brain section (400 μm) using an Olympus BX 51 fluorescence microscope. The distribution of immunolabeled proteins (MAPK/ErK1/ErK2, CaMKII α , GABA, and VGLUT 2) in the PVN were determined using confocal microscopy (Olympus FluoView 10i). To demonstrate cellular changes in inhibitory neurons (Venus) of the PVN, whole brain confocal scans and montaged higher magnification images were generated for (VGAT)-Venus mice after ISOP treatment. Immunolabeled cells and proteins were counted in confocal PVN images ($n = 5$ per group per protein) using Image J (NIH, USA). Furthermore, the average count per unit area was estimated bilaterally relative to the third ventricle. For each PVN on a section, the count was determined for $n = 7$ areas (per μm^2) in different field of views. We determined the limits of the PVN using cellular morphology characterization and region-dependent cell density. This was combined with retrograde tracing (as above) to determine the approximate PVN region projecting to the NTS.

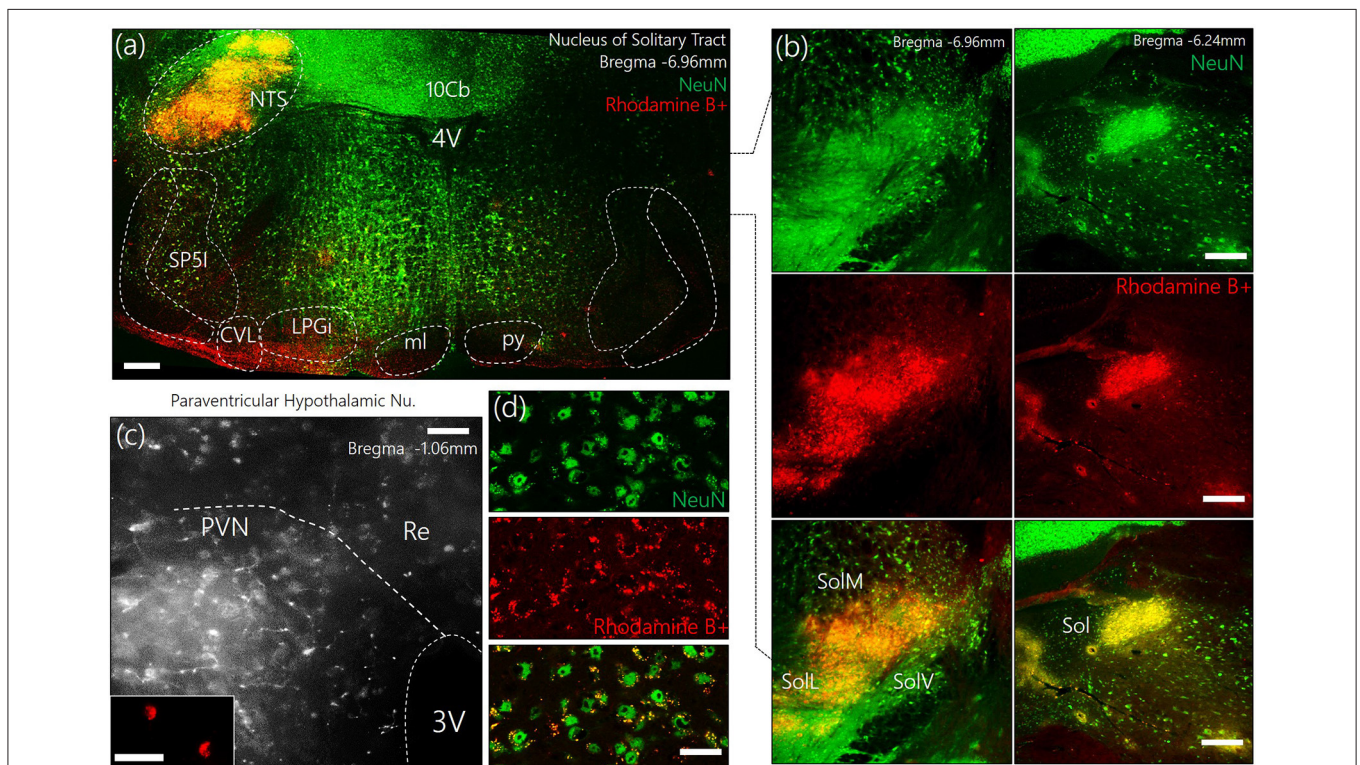
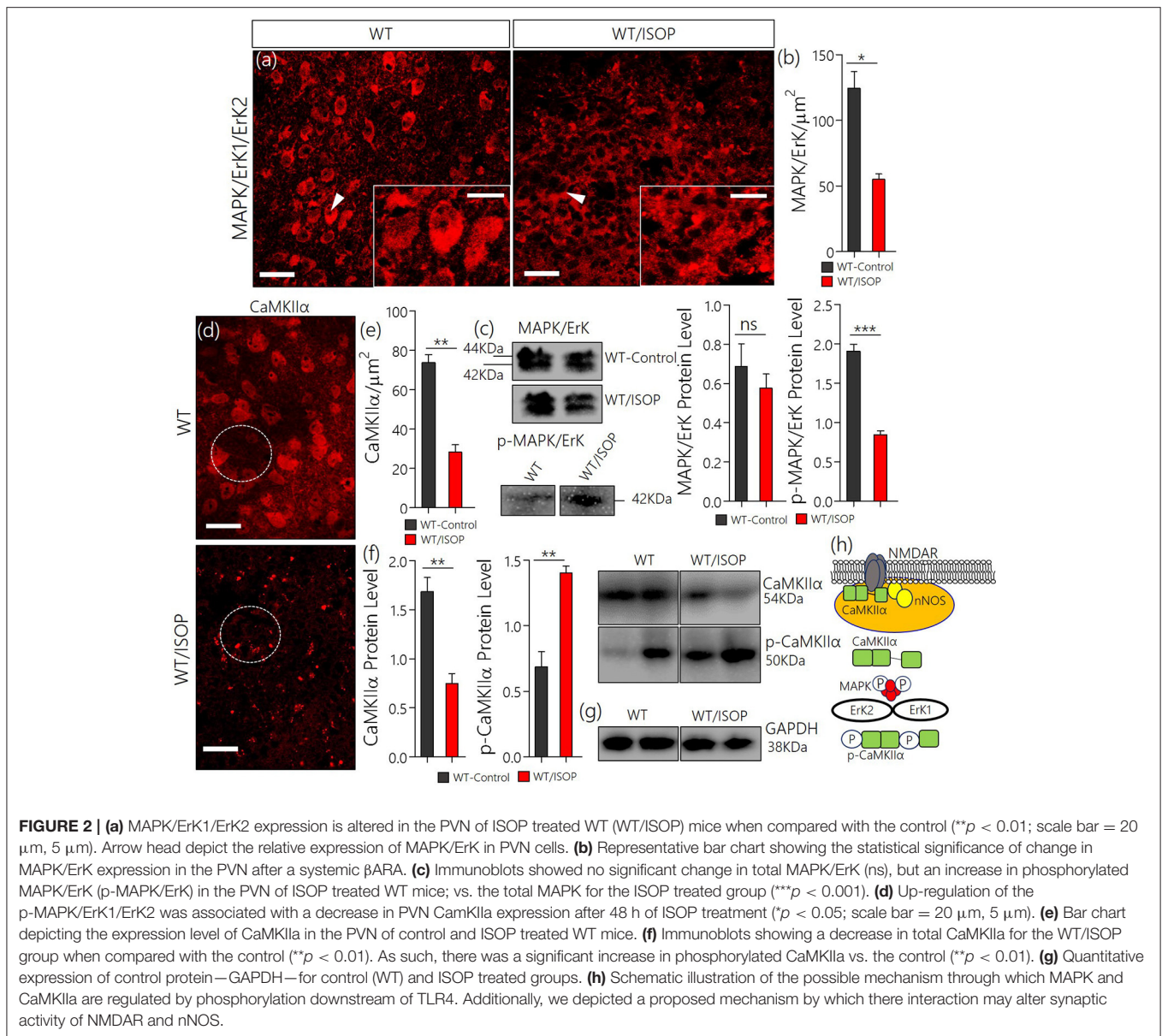


FIGURE 1 | (a) Representative confocal images showing the injection site for the retrograde label—Rhodamine B+ Amine (10,000 MW)—in the Nucleus of tractus solitarius. NTS, Nucleus of tractus solitarius; Sol, Solitary tract (M: Medial, L: Lateral, V: Ventral); SP51, spinal trigeminal nucleus (interpolar part); ml, medial lemniscus; py, pyramidal tract; 4V, fourth ventricle; 10Cb, lobule of 10th cerebellar vermis; CVL, caudoventrrolateral reticular nucleus; LPGI, lateral paragigantocellular nucleus. **(b)** Fluorescence images showing the co-localization of Rhodamine and NeuN (neurons) in the posterior and anterior parts of the Sol (scale bar = 50 μm). **(c)** Confocal images showing the distribution of Rhodamine labelled retrograde vesicles in the PVN after a 7-day survival period (scale bar = 50 μm). (Inset) Localization of Rhodamine in the PVN neurons (scale bar = 30 μm). **(d)** Co-localization of retrograde labels and neurons (NeuN) in the PVN (scale bar = 20 μm).



Statistics

The average values for cell counting per unit area and fluorescence yield were compared for WT vs. WT/ISOP, TLR4^{loxP/loxP}/ISOP vs. TLR4^{Cre/-}/ISOP, and (VGAT)-Venus/ISOP vs. (VGAT)-Venus /Saline (control) mice using Student's *t*-test (GraphPad Prism Version 5). The outcome of statistical analysis was presented in bar chart with error bar representing the mean \pm SEM.

RESULTS

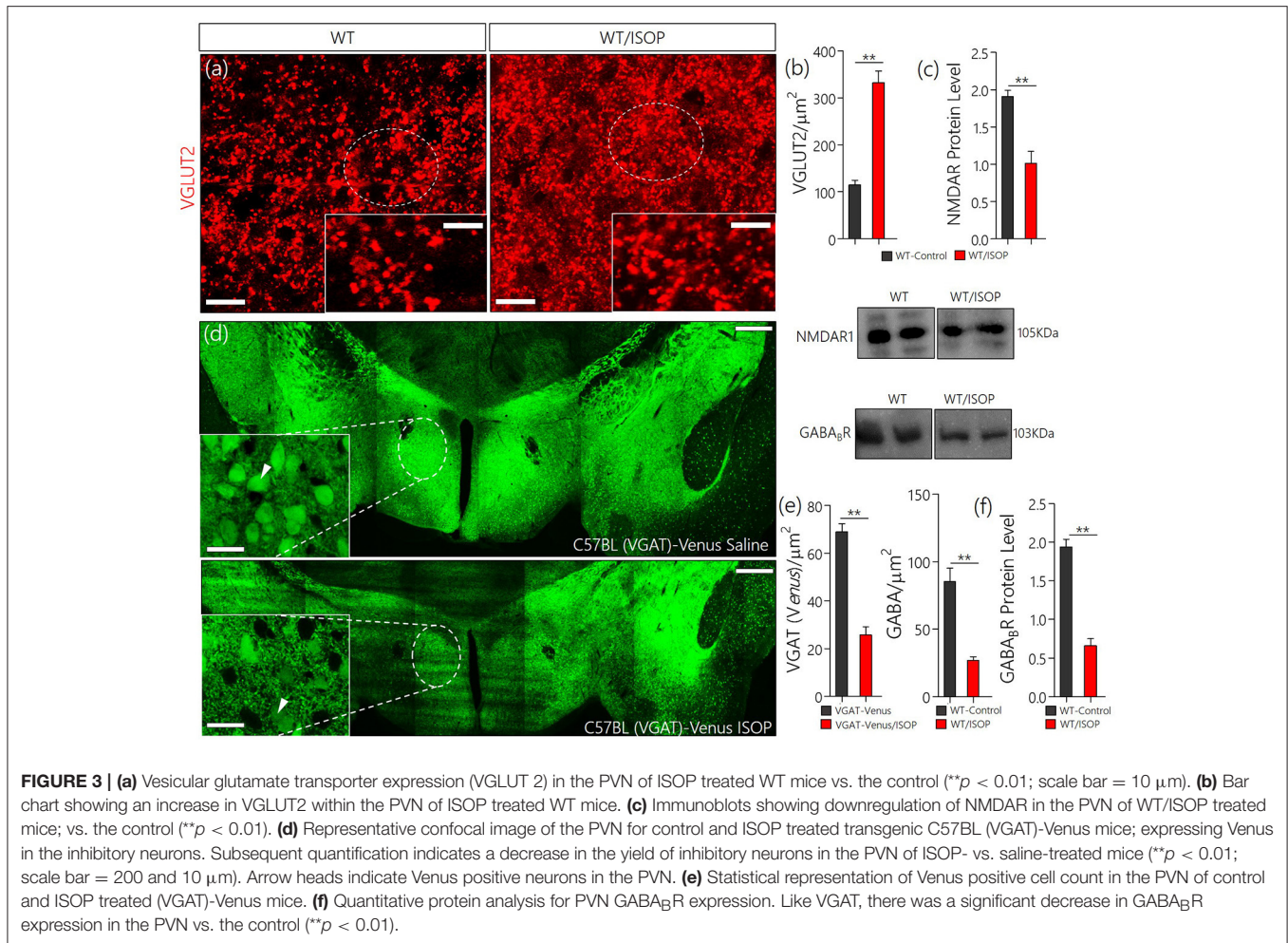
Retrograde Labeling

To identify the approximate localization of pre-autonomic sympathetic neurons, we employed retrograde anatomical tracing methods to outline of the PVN after a dye was injected

into the NTS (Figures 1a,b). The outcome of this experiments showed that retrogradely labeled cells were relatively abundant in the superiomedial aspect of the PVN. As shown in Figures 1c,d, retrograde vesicles were co-localized with neuronal cell bodies labeled with NeuN.

Systemic β ARA Altered Synaptic Kinases Expression in the PVN of WT Mice

After β ARA, in confocal microscopy, we found a significant decrease in total MAPK/Erk expression within the PVN of the WT/ISOP group when compared with the control (Figures 2a,b; $p < 0.05$). However, the expression of phosphorylated MAPK/Erk increased in the WT-ISOP group when compared to the total MAPK expression in quantitative immunoblotting (Figure 2c; $p < 0.05$). Overall, the total MAPK expression



reduced significantly for the WT/ISOP group when compared with the control (Figures 2a–c). Alterations in MAPK/ErK and p-MAPK/ErK were accompanied by a significant loss of CaMKII α in the PVN neurons of ISOP treated mice when compared with the control (Figures 2d,e). Interestingly, in quantitative protein analysis, we recorded a significant decrease in PVN CaMKII α ($p < 0.01$), and an increase in phosphorylated CaMKII α ($p < 0.01$) when the WT/ISOP group was compared with the control (Figures 2f,g). This suggests that a change in systemic sympathetic β ARA elicited neural changes in PVN by altering the expression of pattern of kinases involved in the regulation of synaptic function within the PVN (Figure 2h). Specifically, this involved a preferential expression of p-MAPK/ErK and downregulation of CaMKII α through phosphorylation (increased p-MAPK/ErK).

Systemic β ARA Altered the PVN Glutamate/GABA Expression Pattern

In subsequent experiments we evaluated the significance of changes in MAPK/CaMKII α on components of the PVN glutamate/GABA system. Here we showed the distribution of transporters (VGLUT2 and VGAT) and associated

receptors (NMDAR and GABA_BR) in the PVN of control and ISOP treated mice (WT/ISOP). In addition to a change in MAPK/ErK/CaMKII α , ISOP treated mice showed a significant upregulation of VGLUT 2 (Figures 3a,b; $p < 0.01$), but a decrease in NMDAR expression in the PVN when compared with the control (Figure 3c; $p < 0.01$). In a separate experiment, transgenic (VGAT)-Venus mice, which express the Venus fluorescent protein (an enhanced form of YFP) in inhibitory GABAergic and glycinergic neurons, were treated with ISOP to determine the effect of β ARA on inhibitory neurons in the PVN. A significant decrease in Venus fluorescence intensity was observed in the PVN of ISOP treated (VGAT)-Venus mice when compared with control (VGAT)-Venus group (Figures 3d,e). Furthermore, there was a significant loss of GABA_BR in the PVN ($p < 0.01$; Figure 3f). Based on these outcomes, we deduced that acute systemic β AR activation promotes pre-autonomic glutamatergic vesicular activity, while suppressing inhibitory neurotransmission.

Sympathoexcitation in β AR Activation

Since we have shown that a systemic adrenergic activation may cause certain indirect effects on preautonomic function,

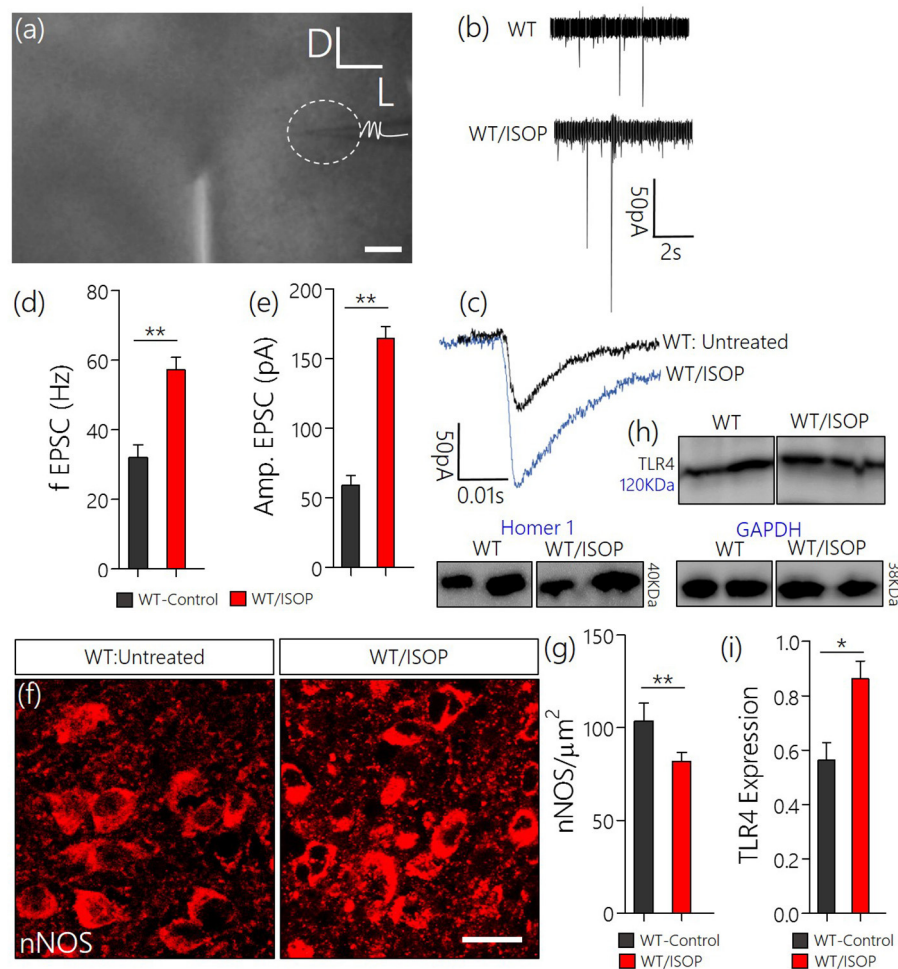


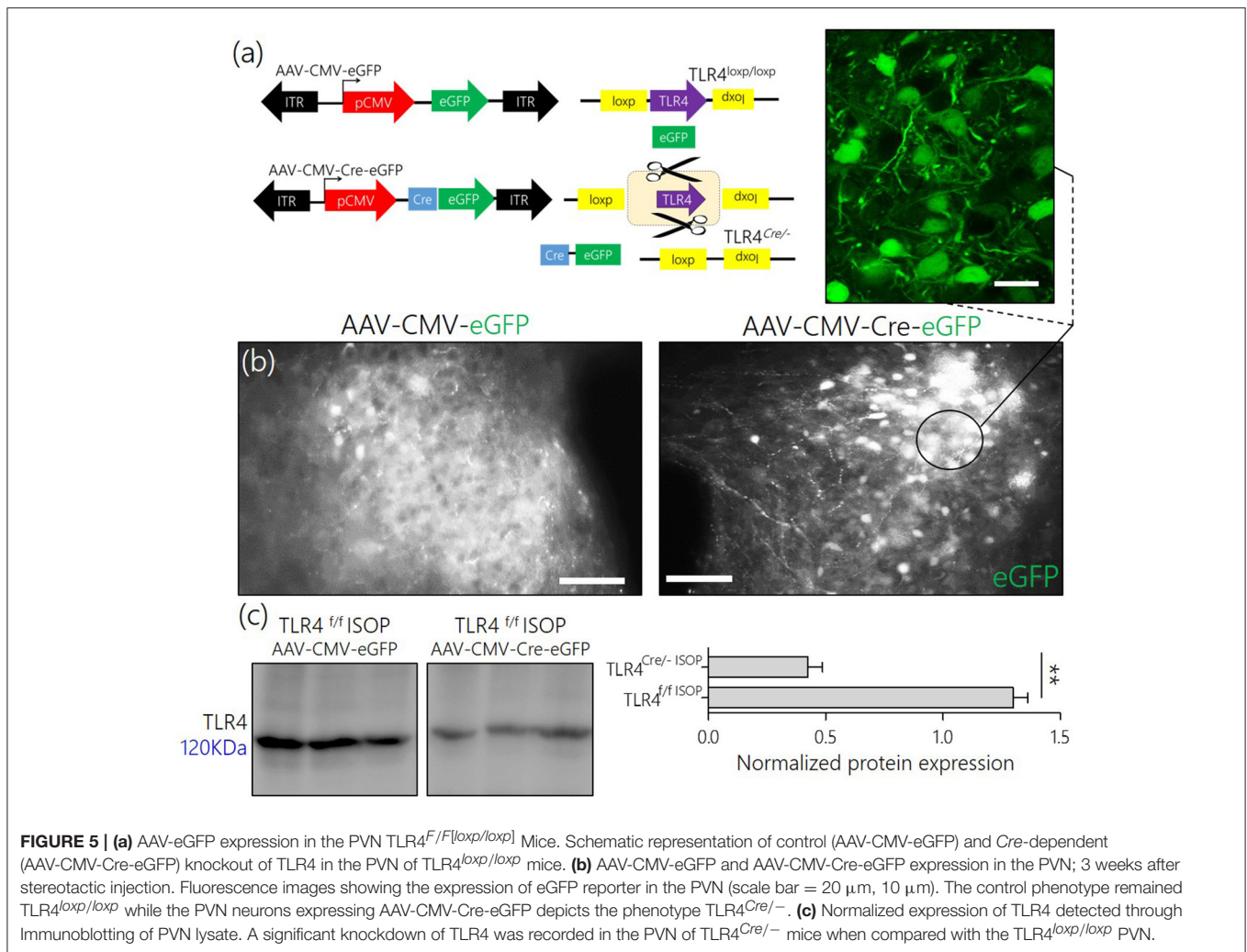
FIGURE 4 | (a) Phase contrast image showing the relative placement of patch pipette electrode in acute slice (PVN) physiology (Scale bar = 100 μm). (b,c) Spontaneous EPSCs recorded from the PVN of control mice, and mice previously treated with ISOP (in vivo). ISOP treated WT mice showed an increase in the frequency (** $p < 0.01$) and amplitude (** $p < 0.01$) of spontaneous EPSCs when compared with control (untreated WT) PVN neurons. (d,e) Bar chart depicting a significant increase in the frequency (** $p < 0.01$) and amplitude (** $p < 0.01$) of EPSCs in the PVN of ISOP treated mice. (f,g) Representative confocal images showing a decrease in nNOS in the PVN after a systemic ISOP treatment (Scale bar = 20 μm). This further supports a change in NMDAR function and synaptic stress after an acute systemic adrenergic activation. (h) In addition to a decrease in nNOS, TLR expression increased in the PVN of WT/ISOP mice (* $p < 0.05$). (i) Bar chart showing the normalized TLR4 expression for control (WT) and WT/ISOP groups.

we verified this observation by determining the profile of spontaneous EPSCs in acute slices prepared from ISOP treated mice (Figure 4a). Using whole-cell perforated patch recordings from the PVN of WT/ISOP group ($n = 5$), we found an increase in spontaneous EPSCs when compared with the control ($p < 0.01$). Additionally, there was an increase in the amplitude of the EPSCs ($p < 0.01$) vs. the control (Figures 4b–e). In support of this outcome, we quantified the expression of nNOS as an indicator of sympathoexcitation that may be related to both NMDAR and GABA_BR function. Interestingly, we found a decrease in nNOS in the PVN of WT/ISOP groups when compared with the control ($p < 0.01$; Figures 4f,g). Ultimately, these changes were associated with an increase in PVN TLR4 expression ($p < 0.05$; Figures 4h,i).

Tissue-Specific Knockdown of PVN TLR4 Reduced Systemic βAR -Mediated MAPK/ErK Expression

From these findings, we hypothesized that an alteration of synaptic kinases may be responsible for the overall change in synaptic function associated with a systemic βARA . Since the balance between CaMKII α and MAPK/ErK expression, and phosphorylation, is involved in inflammatory receptor (TLR4) signaling, we asked whether manipulation of TLR4 in the PVN reduces the threshold of MAPK/CaMKII α imbalance and PVN sympathoexcitation (Figure 5a).

After stereotactic injection of AAV-cocktail in the PVN, successful AAV gene transfection was confirmed through fluorescence detection of the reporter (eGFP) for AAV-CMV-eGFP and AAV-CMV-Cre-eGFP in the PVN after



21 days (**Figure 5b**). To confirm the knockdown of TLR4 in the PVN of $TLR4^{loxp/loxp}$ mice, we estimated TLR4 expression using western blotting analysis. Our results showed a significant reduction in TLR4 expression in untreated $TLR4^{Cre/-}$ when compared with the untreated $TLR4^{loxp/loxp}$ PVN (**Figure 5c**).

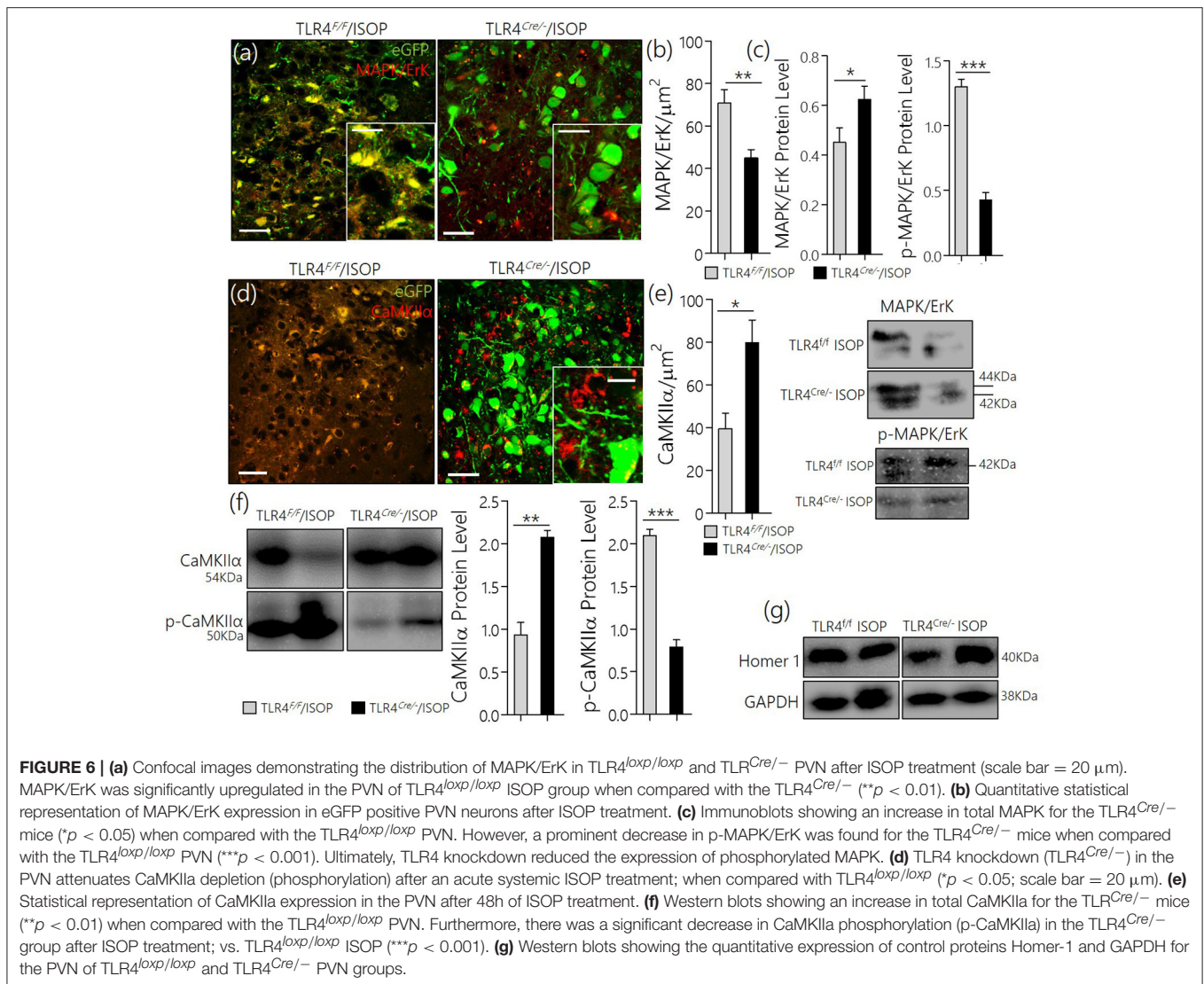
$TLR4^{Cre/-}$ Attenuated MAPK/CaMKII α Imbalance

After knockdown of TLR4, $TLR4^{loxp/loxp}$, and $TLR4^{Cre/-}$ (PVN specific knockdown) mice were treated with ISOP (48 h) following which we evaluated the expression of MAPK/ErK and other associated molecules in the PVN; as described previously in WT. A significant decrease in MAPK/ErK expression was observed in the PVN of $TLR4^{Cre/-}$ mice, after β ARA, when compared with the $TLR4^{loxp/loxp}$ mice ($p < 0.05$) in confocal microscopy (**Figures 6a,b**). In subsequent analysis, using western blotting technique, we showed a significant decrease in p-MAPK/ErK ($p < 0.001$), but not MAPK/ErK ($p < 0.05$) in the PVN of $TLR4^{Cre/-}$ ISOP group; when compared with the $TLR4^{loxp/loxp}$ PVN (**Figure 6c**). The significance of p-MAPK/ErK downregulation in $TLR4^{Cre/-}$ PVN was further verified by

quantitative analysis of CaMKII α in eGFP expressing neurons in $TLR4^{loxp/loxp}$ and $TLR4^{Cre/-}$ PVN. Interestingly, the loss of CaMKII α was significantly attenuated in eGFP positive neurons of $TLR4^{Cre/-}$ and not in $TLR4^{loxp/loxp}$ PVN after ISOP treatment ($p < 0.05$; **Figures 6d,e**). In protein quantification, CaMKII α expression was significantly higher in $TLR4^{Cre/-}$ PVN after ISOP treatment; vs. $TLR4^{loxp/loxp}$ PVN ($p < 0.01$). Evidently, the $TLR4^{loxp/loxp}$ ISOP group recorded a significant increase p-CaMKII α when compared with $TLR4^{Cre/-}$ PVN; which showed less p-CaMKII α ($p < 0.001$; **Figures 6f,g**).

$TLR4^{Cre/-}$ Rescued Inhibitory GABA Neurons and Reduced VGLUT2 in Systemic β ARA

In keeping with the role of TLR4 knockout in the attenuation of MAPK/ErK/CaMKII α imbalance, there was a corresponding reduction of VGLUT2 (**Figures 7a,b**), and an upregulation of NMDAR in the $TLR4^{Cre/-}$ ISOP when compared with the $TLR4^{loxp/loxp}$ PVN (**Figure 7c**). Additionally, our results showed that a change in PVN MAPK/ErK/CaMKII α expression in



$TLR4^{loxp/loxp}$ ISOP group was associated with a decrease in GABA ($p < 0.001$; **Figures 7d,e**) and GABA $_B$ R ($p < 0.01$; **Figures 7f,g**); like the WT/ISOP. However, in the $TLR4^{Cre-/-}$ PVN, after ISOP treatment, GABA and GABA $_B$ R depletion was rescued; vs. the $TLR4^{loxp/loxp}$ PVN (**Figures 7d,g**).

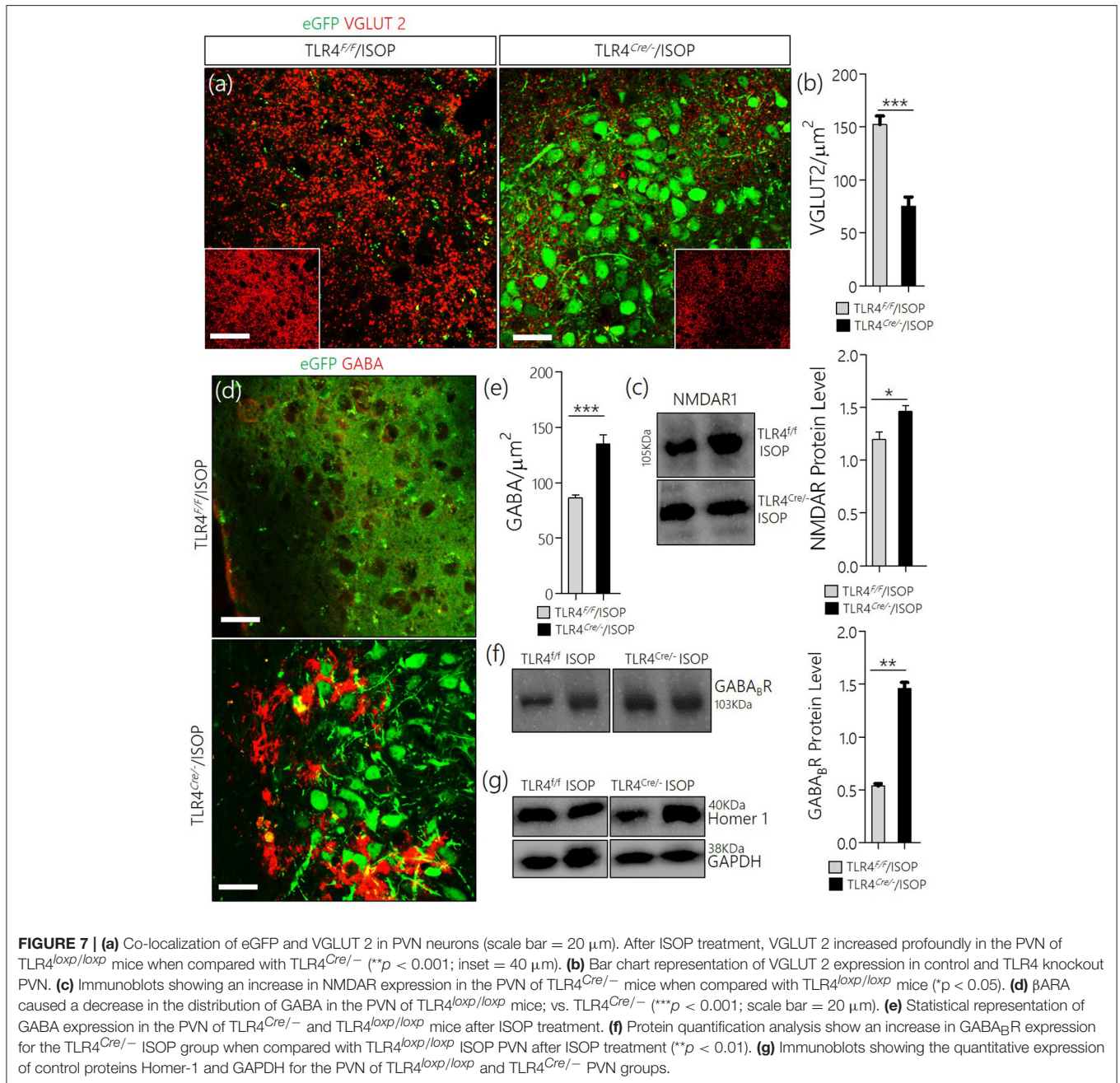
TLR4^{Cre-/-} Reduced Sympathoexcitation in β AR Activation

Similar to the observation in WT/ISOP PVN, $TLR4^{loxp/loxp}$ ISOP PVN neurons showed an increase in the frequency and amplitude of spontaneous EPSCs when compared with the WT control (**Figures 8a,b**). Interestingly, after TLR4 knockout, there was an increase in frequency but not the amplitude of EPSCs in the PVN neuron ($p < 0.01$, ns; **Figures 8c,d**). As a confirmation of a reduction in sympathoexcitation see Sharma et al. (2011), we found that the expression of nNOS was significantly higher for the $TLR4^{Cre-/-}$ ISOP; when compared with the $TLR4^{loxp/loxp}$ ISOP group (**Figure 8e-g**; $p < 0.01$).

Reduced Sympathoexcitation and Cardiac Tissue Morphology

Since TLR4 knockout in the PVN reduced the imbalance between MAPK/ErK and CaMKII α , we sought to elucidate if this contributes to the overall profile of cardiac tissue morphology (histology). After 48 h of ISOP treatment, we confirmed sympathoexcitation by serologically determining the areas affected systemic β ARA in ventricular wall (**Figures 9a,b**). While WT/ISOP and $TLR4^{loxp/loxp}$ ISOP showed significant changes in ventricular wall, no prominent change was recorded in the $TLR4^{Cre-/-}$ ISOP (**Figure 9c**). However, there was an increase in lumen size for the $TLR4^{Cre-/-}$ ISOP group when compared with the control.

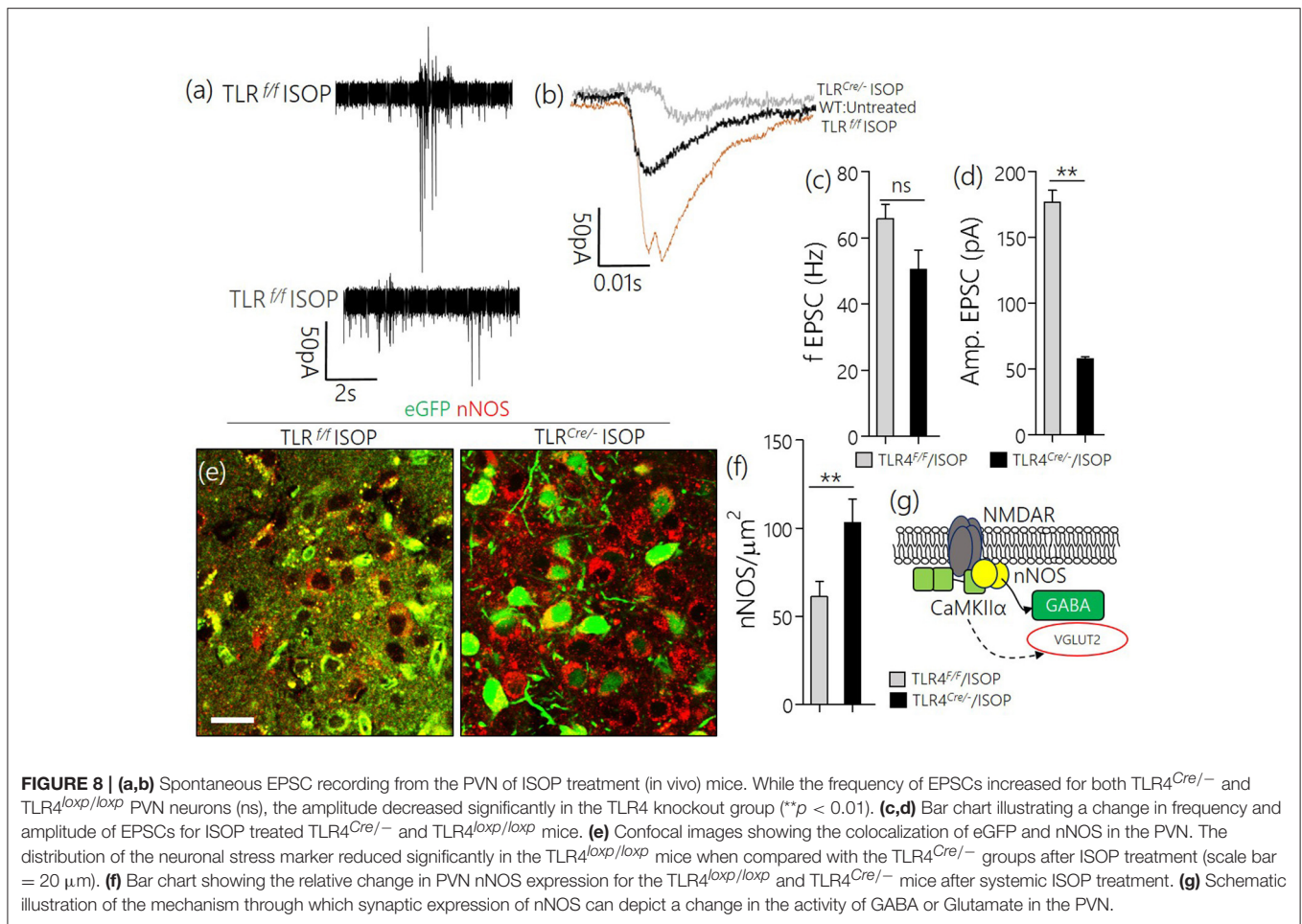
In support of this outcome, we observed increase in cardiac thickness after 48 h of isoproterenol treatment in WT mice as reflected by a significant increase in the thickening of interventricular septum in systole, posterior wall thickness in both systole and diastole. In addition,



WT mice infused with ISO showed an increase in heart rate. In contrast, treatment of TLR4 knockout mice with ISO did not increase ventricular thickness or heart rate. In agreement with echocardiographic finding, histological finding revealed thickening of the wall without an increase in LV cavity size indicating enhanced contraction in WT mice treated with ISO but not in the TLR4 knockout mice. These finding indicate beta adrenergic stimulation increased cardiac contractility and this effect was blunted in TLR4 knockout mice indicating a role for inflammatory molecule in cardiac dysfunction and exaggerated sympathetic activity in mice (Table 1).

DISCUSSION

The outcomes of this study suggest that systemically driven βARA causes a change in phosphorylation and expression of synaptic kinases (MAPK/ErK/CaMKII α) in the PVN. This was generally associated with a significant increase in p-MAPK/ErK, and phosphorylation of synaptic regulatory kinase (CaMKII α). Furthermore, there was a change in the distribution of transporter and receptor components of Glutamate/GABA neurotransmission within the PVN after an acute—*in vivo*—systemic ISOP treatment. Taken together, we showed that pertaining to an acute systemic βARA , an upregulation of



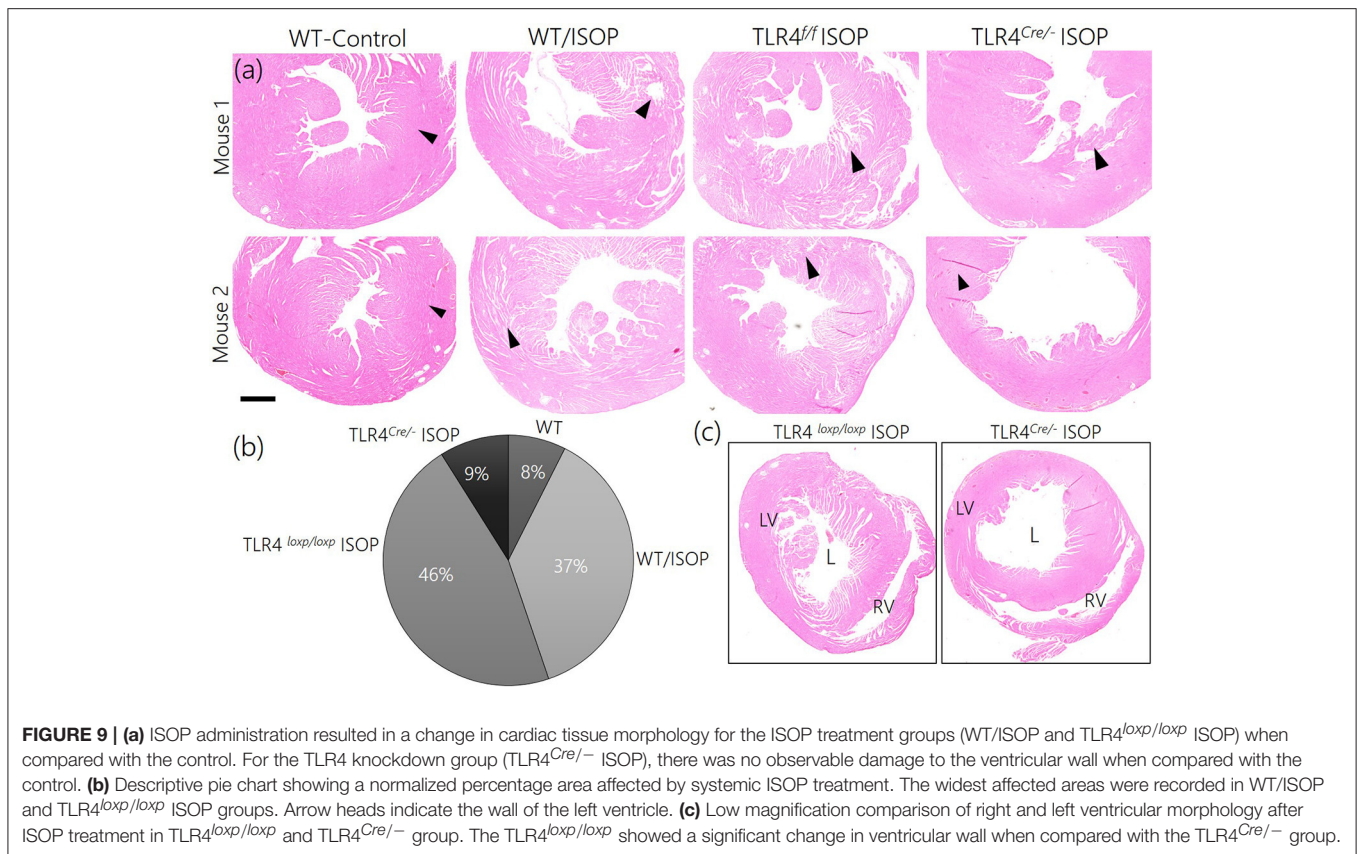
PVN p-CaMKII α , and associated neurochemical changes were mediated—in part—through the neural MAPK/TLR4 axis. As such, a change in PVN MAPK/ErK/CaMKII α phosphorylation pattern may be central to the synaptic changes observed in response to systemic β ARA.

MAPK/ErK signaling is an integral part of TLR4 activation associated with neuroinflammatory responses in the CNS (Badshah et al., 2016; Cho et al., 2016). Furthermore, MAPK/ErK activation, downstream of TLR4, may contribute to the phosphorylation (inactivation) of CaMKII α at post-synaptic sites (Liu et al., 2010; Li et al., 2015). Recent studies have described the role of neural inflammation in systemic cardiovascular changes. Moreover, there is substantive evidence to suggest that deletion of cardiac TLR4 is protective against systemic ISOP-induced necrosis (Kim et al., 2006). Yet, it has been unclear whether a systemic driven change in cardiovascular function can directly alter PVN synaptic function.

The PVN has initially been described as a mere relay station for neurons of the descending hypothalamic-hypophysial systems (Babović et al., 2009). However, morphological and electrophysiological characterization of PVN neurons shows that it is made up of several integrated excitatory and inhibitory neural circuits concerned with the regulation of autonomic cardiovascular functions (Pyner, 2009; Glass et al., 2015; Pandit et al., 2015; Ogundele et al., 2016a). An important component

of the pre-autonomic sympathetic control is the activity of adrenergic neurotransmitters in parts of the brain connected to the PVN (Jung et al., 2004). Specifically, the rostral ventrolateral medulla (RVLM), NTS, and catecholaminergic neuron group (C1) of the brain stem receives autonomic inputs from the PVN and projects to the intermediolateral column of the spinal cord (thoracolumbar region). This then innervates the heart through the cardiac plexus (Menani et al., 2014; Van Kempen et al., 2015; Ogundele et al., 2016b).

Physiologically, the state of the excitatory and inhibitory neurotransmitters, within the PVN, is an indirect representation of the magnitude of sympathoexcitation (Zhang et al., 2002; Li and Pan, 2007). While a systemic β AR activation may increase the heart rate by stimulating β 2 receptors in the heart (Yusuf et al., 1987), the outcome of this study suggests that such an activation may alter pre-autonomic events. As such, since ISOP does not readily cross the blood-brain barrier (Olesen et al., 1978), it is logical to assume that the changes observed here were to a large extent part of a wide and diffuse response to cardiac mechanical receptor activation, rather than β 2R signaling within the PVN. Interestingly, this effect may occur in reverse. As such, neural factors which promotes excitatory activity, or decrease inhibitory neurotransmission in the PVN has been shown to increase sympathoexcitation (Patel et al., 2016).

**TABLE 1 |** Values are means \pm SE.

Parameters	Exp. groups	Baseline	48 h
IVSd (mm)	WT+ISO	0.70 \pm 0.02	0.77 \pm 0.01
	$TLR4$ +ISO	0.74 \pm 0.01	0.76 \pm 0.01
IVSs (mm)	WT+ISO	1.03 \pm 0.02	1.22 \pm 0.02*
	$TLR4$ +ISO	1.04 \pm 0.01 [#]	0.97 \pm 0.01 ^{\$}
LVIDd (mm)	WT+ISO	3.70 \pm 0.02	3.77 \pm 0.03
	$TLR4$ +ISO	3.74 \pm 0.03	3.84 \pm 0.03
LVIDs (mm)	WT+ISO	2.32 \pm 0.01	2.30 \pm 0.02
	$TLR4$ +ISO	2.34 \pm 0.01	2.33 \pm 0.01
LVPWd (mm)	WT+ISO	0.77 \pm 0.01	0.87 \pm 0.01
	$TLR4$ +ISO	0.74 \pm 0.01	0.78 \pm 0.01 ^{\$}
LVPWs (mm)	WT+ISO	1.15 \pm 0.03	1.37 \pm 0.02*
	$TLR4$ +ISO	1.08 \pm 0.03 [#]	1.13 \pm 0.01 ^{\$}
FS (%)	WT+ISO	35.68 \pm 0.71	37.52 \pm 0.33
	$TLR4$ +ISO	35.68 \pm 0.45	36.14 \pm 0.24
HR	WT+ISO	479.0 \pm 4.81	584.79 \pm 7.98*
	$TLR4$ +ISO	487.4 \pm 6.85 ^{#&}	510.20 \pm 5.35 [@]

IVSd and IVDs, interventricular septal thickness in diastole and systole, respectively; LVIDd and LVIDs indicate left ventricular internal diameter at diastole and systole, respectively; LVPWd and LVPWs, left ventricular posterior wall thickness at diastole and systole, respectively; FS, fractional shortening and HR, heart rate.

$p < 0.05$ -WT - Baseline vs. WT + ISO 48 h*, $p < 0.05$ -WT + ISO 48 h^{\$} vs. $TLR4KO$ - Baseline[#], $p < 0.05$ -WT + ISO 48 h vs. $TLR4KO$ - 48 h^{\$}, $p < 0.05$ -WT Baseline vs. $TLR4KO$ - 48 h[&], $p < 0.05$ -WT + ISO 48 h vs. $TLR4KO$ - Baseline[#], and $p < 0.05$ -WT + ISO 48 h vs. $TLR4KO$ - 48h[@].

Data were submitted to multivariate analysis of variance (MANOVA) and then compared between groups and moments by Tukey-Cramer.

Substantive evidence now exists to suggest that β_2R activation generates a significant level of MAPK/ErK in the tissue through the cyclic adenosine monophosphate/protein kinase A signaling pathways (Zheng et al., 2000). Other studies have shown a direct relationship between the release of calcium and MAPK generated after β_2R activation in cardiomyocytes (Magne et al., 2001). Aside from their role in the regulation of synaptic dysfunction and calcium release, the MAPK and CaMKII α are also involved in inflammatory signaling downstream of $TLR4$ (Wang et al., 2014; Swaroop et al., 2016). Since MAPK/ErK is a major signaling molecule acting downstream of $TLR4$, we asked whether targeting PVN $TLR4$ may attenuate some of the neurochemical changes associated with systemic βAR activation-mediated MAPK/CaMKII α imbalance. Like the observation in cardiac tissue, the outcome of this study showed that $TLR4$ knockout attenuates PVN MAPK/ErK phosphorylation (Figures 6a-c) after an acute systemic βAR activation when compared with the WT. Furthermore, this prevented loss of CaMKII α , and restored excitatory/inhibitory neurotransmitter balance (Figures 6d-f). The significance of a change in MAPK/ErK expression in eGFP positive neurons for $TLR4^{Cre/-}$ -ISOP (Figure 6a) vs. its expression in PVN total lysate (Figure 6b) cannot be over emphasized. While we have highlighted the expression of MAPK/ErK co-localized with eGFP in microscopy, these images did not highlight possible changes in astroglia MAPK/ErK or p-MAPK/ErK. However, in immunoblots, all sources of MAPK/ErK and p-MAPK/ErK were considered.

To determine the relationship between CaMKII α and TLR4 expression patterns, we quantified total MAPK/ErK and, phosphorylated MAPK/ErK in the PVN of ISOP treated mice. Although there was an increase in total MAPK/ErK in PVN total lysate (**Figure 6b**; $p < 0.05$), confocal imaging revealed a decrease in MAPK/ErK—specifically—for eGFP positive PVN neurons in TLR4^{Cre/-}-ISOP group (**Figure 6a**; $p < 0.01$). Since it has been established that p-MAPK/ErK phosphorylates CaMKII α (Mizukami et al., 2015; Yu et al., 2016), we further quantified the expression of PVN p-MAPK/ErK in the PVN. Although TLR4^{Cre/-}-ISOP group recorded a higher PVN MAPK/ErK expression, there was a significant decrease in p-MAPK/ErK when compared with the TLR4^{loxP/loxP} ISOP group ($p < 0.001$) after ISOP treatment. In subsequent analysis, we deduced that these outcomes may hold a direct effect of CaMKII α expression and phosphorylation pattern. As such, a decrease in p-MAPK/ErK in the PVN of TLR4^{Cre/-}-ISOP group was associated with an increased expression of CaMKII α ($p < 0.01$), but not p-CaMKII α when compared to the TLR4^{loxP/loxP} ISOP group—which showed the opposite (**Figures 6d–f**).

TLR4 Knockout Attenuated Sympathoexcitation in β ARA

Here we showed that an acute β AR activation was associated with alterations in preautonomic synaptic substrates. This was generally accounted for a change in glutamatergic and GABAergic systems (**Figure 2**). Although VGLUT2 expression increased in the preautonomic area, there was a significant decrease in NMDAR expression in the PVN of ISOP treated mice. However, a striking decrease in VGAT/GABA and GABA_BR suggests a decreased inhibition of the PVN during an acute systemic ISOP treatment. In support of this proposition, a decrease in GABA and GABA_BR was associated with an increased threshold and frequency for spontaneous EPSCs in the preautonomic area (**Figure 4**).

TLR4 may alter the expression of nNOS through the activity of MAPK/ErK at synaptic densities (Yao et al., 2012; Wang et al., 2016). Moreover, a reduction in the expression of nNOS, during inflammation, has been described in the loss of NO and GABA activity (Lethbridge et al., 2012; Di Mauro et al., 2013). Ultimately, our results showed that an increase in sympathoexcitation may involve MAPK-mediated glutamatergic activity or nNOS-related GABA loss after β ARA. While nNOS is required for NO-mediated GABAergic activation, a reduction in the tissue level of NO and GABA has been described in the PVN after a phase of TLR4-mediated inflammation (Affleck et al., 2012). Furthermore, the activity of downstream pro-inflammatory molecules—such as NF- κ B and IL-1 β —have been identified in nNOS/GABA inhibition in the PVN (Crowley et al., 2015; Dange et al., 2015). Based on our results, and reports by other groups (Kim et al., 2006; Dange et al., 2015; Crowley et al., 2015), we deduced that β ARA caused sympathoexcitation, in part, through TLR4/MAPK/ErK-mediated loss of GABA activity in the PVN. As such, when a tissue—specific TLR4 knockdown was implemented, we observed no significant loss in GABA and nNOS expression in the PVN (TLR4^{Cre/-}) after ISOP treatment. TLR4 knockdown also had a significant effect on the amplitude, but not the frequency of EPSCs in the PVN. As such,

there was no significant change in fEPSC, while the TLR4^{Cre/-}-ISOP responses exhibited a lower threshold vs. TLR4^{loxP/loxP} ISOP.

It is noteworthy to mention that methods such as RT-PCR can serve as useful tools in adequately measuring the extent of knockdown attained using the AAV cocktail and protein expression. However, western blotting gave us an overall outcome on protein expression pattern. This was ultimately used to determine the extent of the knockdown in PVN lysate. While our study has opened a new premise for assessing the crosstalk between PVN synaptic kinases and systemic cardiovascular activation, there are several gaps that our study does not address. Majorly, since ISOP remains systemic thereafter, the actual mechanism through which these changes may occur remains open for further investigation. A logical explanation may involve a broad up-regulation of p-MAPK (systemic) capable of causing changes in blood vessels, and permeability of the blood brain barrier (González-Mariscal et al., 2008; Pan et al., 2011). Additionally, systemic ISOP treatment may involve neural stress response mechanism—through adrenergic systems—and oxidative stress (Rathore et al., 2000) that is capable of eliciting changes in the PVN. Therefore, there is a need for further characterization of stress response systems, and determining the profile of the blood-brain barrier after acute ISOP treatment.

SUMMARY

Although systemic ISOP does not effectively cross the blood-brain barrier, we found that acute systemic β AR activation may indirectly affect the neurochemical balance of the pre-autonomic PVN through changes in CaMKII α /MAPK/ErK, downstream of TLR4. Consequently, truncating the TLR4 pathway attenuated CaMKII α loss, and restored excitatory/inhibitory neurotransmitter balance to certain extent.

AUTHOR CONTRIBUTIONS

OO, FR, and RD: Conducted aspects of the experiment, analysis and manuscript write up. CL: Supervised the research, conducted aspects of the experiments and revised the manuscript. JF, CL, and RD: Supervised aspect of the research design and implementation, contributed in analysis and edited the final write up.

FUNDING

This study was supported by the IBRO-ISN Fellowship 2015 awarded to OO. NIH Grant R03 MH 104851 and Louisiana Board of Regents RCS Grant RD-A-09 awarded to CL. American Heart Association, Grant-in-Aid: 16GRNT30510012 for Joseph Francis.

SUPPLEMENTARY MATERIAL

The Supplementary Material for this article can be found online at: <http://journal.frontiersin.org/article/10.3389/fnins.2017.00447/full#supplementary-material>

REFERENCES

- Affleck, V. S., Coote, J. H., and Pyner, S. (2012). The projection and synaptic organisation of NTS afferent connections with presympathetic neurons, GABA and nNOS neurons in the paraventricular nucleus of the hypothalamus. *Neuroscience* 219, 48–61. doi: 10.1016/j.neuroscience.2012.05.070
- Babović, S. S., Ivanov, D., Mijatov-Ukropina, L., Toyonaga, T., Dimitrijević, I., and Dordević, M. (2009). Cytoarchitecture of the human paraventricular hypothalamic nucleus. *Med. Pregl.* 62, 417–420. doi: 10.2298/MPNS0910417B
- Badshah, H., Ali, T., and Kim, M. O. (2016). Osmotin attenuates LPS-induced neuroinflammation and memory impairments via the TLR4/NFκB signaling pathway. *Sci. Rep.* 6:24493. doi: 10.1038/srep24493
- Cho, K. H., Kim, D. C., Yoon, C. S., Ko, W. M., Lee, S. J., Sohn, J. H., et al. (2016). Anti-neuroinflammatory effects of citreohybridonol involving TLR4-MyD88-mediated inhibition of NF-κB and MAPK signaling pathways in lipopolysaccharide-stimulated BV2 cells. *Neurochem. Int.* 95, 55–62. doi: 10.1016/j.neuint.2015.12.010
- Crowley, T., Fitzpatrick, J. M., Kuijper, T., Cryan, J. F., O'Toole, O., O'Leary, O. F., et al. (2015). Modulation of TLR3/TLR4 inflammatory signaling by the GABAB receptor agonist baclofen in glia and immune cells: relevance to therapeutic effects in multiple sclerosis. *Front. Cell Neurosci.* 9:284. doi: 10.3389/fncel.2015.00284
- Dange, R. B., Agarwal, D., Masson, G. S., Vila, J., Wilson, B., Nair, A., et al. (2014). Central blockade of TLR4 improves cardiac function and attenuates myocardial inflammation in angiotensin II-induced hypertension. *Cardiovasc. Res.* 103, 17–27. doi: 10.1093/cvr/cvu067
- Dange, R. B., Agarwal, D., Teruyama, R., and Francis, J. (2015). Toll-like receptor 4 inhibition within the paraventricular nucleus attenuates blood pressure and inflammatory response in a genetic model of hypertension. *J. Neuroinflammation.* 12, 31. doi: 10.1186/s12974-015-0242-7
- Dawaliby, R., Trubbia, C., Delporte, C., Masureel, M., Van Antwerpen, P., Kobilka, B. K., et al. (2016). Allosteric regulation of G protein-coupled receptor activity by phospholipids. *Nat. Chem. Biol.* 12, 35–39. doi: 10.1038/nchembio.1960
- Di Mauro, M., Li Volsi, G., and Licata, F. (2013). Noradrenergic control of neuronal firing in cerebellar nuclei: modulation of GABA responses. *Cerebellum* 12, 350–361. doi: 10.1007/s12311-012-0422-2
- Fischer, A. H., Jacobson, K. A., Rose, J., and Zeller, R. (2008). Hematoxylin and eosin staining of tissue and cell sections. *CSH Protoc.* doi: 10.1101/pdb.prot4986. [Epub ahead of print].
- Franklin, K., and Paxinos, G. (1997). *The Mouse Brain in Stereotaxic Coordinates*. San Diego, CA: Academic Press, 45–56.
- Giudice, P. L., Bonomini, M., and Arduini, A. (2016). A moderate carnitine deficiency exacerbates isoproterenol-induced myocardial injury in rats. *Cardiovasc Drugs Ther.* 30, 119–127. doi: 10.1007/s10557-016-6647-4
- Glass, M. J., Wang, G., Coleman, C. G., Chan, J., Ogorodnik, E., Van Kempen, T. A., et al. (2015). NMDA receptor plasticity in the hypothalamic paraventricular nucleus contributes to the elevated blood pressure produced by angiotensin II. *J. Neurosci.* 35, 9558–9567. doi: 10.1523/JNEUROSCI.2301-14.2015
- González-Mariscal, L., Tapia, R., and Chamorro, D. (2008). Crosstalk of tight junction components with signaling pathways. *Biochim. Biophys. Acta* 1778, 729–756. doi: 10.1016/j.bbame.2007.08.018
- Gupta, P., Kanwal, A., Putcha, U. K., Bulani, Y., Sojitra, B., Khatua, T. N., et al. (2013). Cardioprotective effect of ritonavir, an antiviral drug, in isoproterenol induced myocardial necrosis: a new therapeutic implication. *J. Transl. Med.* 11:80. doi: 10.1186/1479-5876-11-80
- Ichikawa, O., Fujimoto, K., Yamada, A., Okazaki, S., and Yamazaki, K. (2016). G-Protein/β-arrestin-linked fluctuating network of G-protein-coupled receptors for predicting drug efficacy and bias using short-term molecular dynamics simulation. *PLoS ONE* 11:e0155816. doi: 10.1371/journal.pone.0155816
- Jung, J. Y., Lee, J. U., and Kim, W. J. (2004). Enhanced activity of central adrenergic neurons in two-kidney, one clip hypertension in Sprague-Dawley rats. *Neurosci Lett.* 369, 14–18. doi: 10.1016/j.neulet.2004.07.029
- Kim, N., Kim, H., Youm, J. B., Park, W. S., Warda, M., Ko, J. H., et al. (2006). Site specific differential activation of ras/raf/ERK signaling in rabbit isoproterenol-induced left ventricular hypertrophy. *Biochim. Biophys. Acta* 1763, 1067–1075. doi: 10.1016/j.bbamer.2006.08.002
- Lee, D., Creed, M., Jung, K., Stefanelli, T., Wendler, D. J., Oh, W. C., et al. (2017). Temporally precise labeling and control of neuromodulatory circuits in the mammalian brain. *Nat. Methods* 14, 495–503. doi: 10.1038/nmeth.4234
- Lee, S. K., Ryu, P. D., and Lee, S. Y. (2013). Differential distributions of neuropeptides in hypothalamic paraventricular nucleus neurons projecting to the rostral ventrolateral medulla in the rat. *Neurosci. Lett.* 556, 160–165. doi: 10.1016/j.neulet.2013.09.070
- Lethbridge, R., Hou, Q., Harley, C. W., and Yuan, Q. (2012). Olfactory bulb glomerular NMDA receptors mediate olfactory nerve potentiation and odor preference learning in the neonate rat. *PLoS ONE* 7:e35024. doi: 10.1371/journal.pone.0035024
- Li, D. P., and Pan, H. L. (2007). Glutamatergic inputs in the hypothalamic paraventricular nucleus maintain sympathetic vasomotor tone in hypertension. *Hypertension* 49, 916–925. doi: 10.1161/01.HYP.0000259666.99449.74
- Li, Y., Korgaonkar, A. A., Swietek, B., Wang, J., Elgammal, F. S., Elkabes, S., et al. (2015). Toll-like receptor 4 enhancement of non-NMDA synaptic currents increases dentate excitability after brain injury. *Neurobiol. Dis.* 74, 240–253. doi: 10.1016/j.nbd.2014.11.021
- Liu, X., Zhan, Z., Xu, L., Ma, F., Li, D., Guo, Z., et al. (2010). MicroRNA-148/152 impair innate response and antigen presentation of TLR-triggered dendritic cells by targeting CaMKIIα. *J. Immunol.* 185, 7244–7251. doi: 10.4049/jimmunol.1001573
- Lu, H., Tian, A., Wu, J., Yang, C., Xing, R., Jia, P., et al. (2014). Danshensu inhibits β-adrenergic receptors-mediated cardiac fibrosis by ROS/p38 MAPK axis. *Biol. Pharm. Bull.* 37, 961–967. doi: 10.1248/bpb.b13-00921
- Madamanchi, A. (2007). β-Adrenergic receptor signaling in cardiac function and heart failure. *McGill J. Med.* 10, 99–104.
- Magne, S., Couchie, D., Pecker, F., and Pavoine, C. (2001). Beta(2)-adrenergic receptor agonists increase intracellular free Ca²⁺ concentration cycling in ventricular cardiomyocytes through p38 and p42/44 MAPK-mediated cytosolic phospholipase A(2) activation. *J. Biol. Chem.* 276, 39539–39548. doi: 10.1074/jbc.M100954200
- Menani, J. V., Vieira, A. A., Colombari, D. S. A., De Paula, P. M., Colombari, E., and De Luca, L. A. Jr. (2014). “Preoptic–periventricular integrative mechanisms involved in behavior, fluid–electrolyte balance, and pressor responses,” in *Neurobiology of Body Fluid Homeostasis: Transduction and Integration*, eds L. A. De Luca, J. V. Menani, and A. K. Johnson (Boca Raton, FL: CRC Press; Taylor & Francis), Chapter 4.
- Mizukami, K., Yoshikishi, H., Mitsuyama, H., Watanabe, M., Tenma, T., Takada, S., et al. (2015). Small-conductance Ca²⁺-activated K⁺ current is upregulated via the phosphorylation of CaMKII in cardiac hypertrophy from spontaneously hypertensive rats. *Am. J. Physiol. Heart Circ. Physiol.* 309, H1066–H1074. doi: 10.1152/ajpheart.00825.2014
- Mo, G. L., Li, Y., Du, R. H., Dai, D. Z., Cong, X. D., and Dai, Y. (2014). Isoproterenol induced stressful reactions in the brain are characterized by inflammation due to activation of NADPH oxidase and ER stress: attenuated by Apocynin, Rehmannia complex and Triterpene acids. *Neurochem. Res.* 39, 719–730. doi: 10.1007/s11064-014-1260-z
- Morioka, N., Abe, H., Araki, R., Matsumoto, N., Zhang, F. F., Nakamura, Y., et al. (2014). A β1/2 adrenergic receptor-sensitive intracellular signaling pathway modulates CCL2 production in cultured spinal astrocytes. *J. Cell Physiol.* 229, 323–332. doi: 10.1002/jcp.24452
- Ogundele, O. M., Lee, C. C., and Francis, J. (2016a). Age-dependent alterations to paraventricular nucleus insulin-like growth factor 1 receptor as a possible link between sympathoexcitation and inflammation. *J. Neurochem.* 139, 706–721. doi: 10.1111/jnc.13842
- Ogundele, O. M., Lee, C. C., and Francis, J. (2016b). Thalamic dopaminergic neurons project to the paraventricular nucleus-rostral ventrolateral medulla/CI neural circuit. *Anat. Rec.* 300, 1307–1314. doi: 10.1002/ar.23528
- Olesen, J., Hougård, K., and Hertz, M. (1978). Isoproterenol and propranolol: ability to cross the blood-brain barrier and effects on cerebral circulation in man. *Stroke* 9, 344–349. doi: 10.1161/01.STR.9.4.344
- Pan, W., Stone, K. P., Hsueh, H., Manda, V. K., Zhang, Y., and Kastin, A. J. (2011). Cytokine signaling modulates blood-brain barrier function. *Curr. Pharm. Des.* 17, 3729–3740. doi: 10.2174/138161211798220918
- Pandit, S., Jo, J. Y., Lee, S. U., Lee, Y. J., Lee, S. Y., Ryu, P. D., et al. (2015). Enhanced astroglial GABA uptake attenuates tonic GABA_A inhibition of the presympathetic hypothalamic paraventricular nucleus neurons in heart failure. *J. Neurophysiol.* 114, 914–926. doi: 10.1152/jn.00080.2015

- Patel, K. P., Xu, B., Liu, X., Sharma, N. M., and Zheng, H. (2016). Renal denervation improves exaggerated sympathoexcitation in rats with heart failure: a role for neuronal nitric oxide synthase in the paraventricular nucleus. *Hypertension* 68, 175–184. doi: 10.1161/HYPERTENSIONAHA.115.06794
- Pyner, S. (2009). Neurochemistry of the paraventricular nucleus of the hypothalamus: implications for cardiovascular regulation. *J. Chem. Neuroanat.* 38, 197–208. doi: 10.1016/j.jchemneu.2009.03.005
- Ranjan, R., Gupta, P., and Shukla, A. K. (2016). GPCR Signaling: β -arrestins kiss and remember. *Curr. Biol.* 26, R285–R288. doi: 10.1016/j.cub.2016.02.056
- Rathore, N., Kale, M., John, S., and Bhatnagar, D. (2000). Lipid peroxidation and antioxidant enzymes in isoproterenol induced oxidative stress in rat erythrocytes. *Indian J. Physiol. Pharmacol.* 44, 161–166. doi: 10.1006/phrs.1998.0365
- Romberger, D. J., Heires, A. J., Nordgren, T. M., Poole, J. A., Toews, M. L., West, W. W., et al. (2016). Beta-2 adrenergic agonists attenuate organic dust-induced lung inflammation. *Am. J. Physiol. Lung Cell. Mol. Physiol.* 311, L101–L110. doi: 10.1152/ajplung.00125.2016
- Sharma, N. M., Zheng, H., Mehta, P. P., Li, Y. F., and Patel, K. P. (2011). Decreased nNOS in the PVN leads to increased sympathoexcitation in chronic heart failure: role for CAPON and Ang. II. *Cardiovasc. Res.* 92, 348–357. doi: 10.1093/cvr/cvr217
- Swaroop, S., Sengupta, N., Suryawanshi, A. R., Adlakha, Y. K., and Basu, A. (2016). HSP60 plays a regulatory role in IL-1 β -induced microglial inflammation via TLR4-p38 MAPK axis. *J. Neuroinflammation.* 13, 27. doi: 10.1186/s12974-016-0486-x
- Theccanat, T., Philip, J. L., Razzaque, A. M., Ludmer, N., Li, J., Xu, X., et al. (2016). Regulation of cellular oxidative stress and apoptosis by G protein-coupled receptor kinase-2; The role of NADPH oxidase 4. *Cell Signal.* 28, 190–203. doi: 10.1016/j.cellsig.2015.11.013
- Van Kempen, T. A., Dodos, M., Woods, C., Marques-Lopes, J., Justice, N. J., Iadecola, C., et al. (2015). Sex differences in NMDA GluN1 plasticity in rostral ventrolateral medulla neurons containing corticotropin-releasing factor type 1 receptor following slow-pressor angiotensin II hypertension. *Neuroscience* 307, 83–97. doi: 10.1016/j.neuroscience.2015.08.029
- Wang, Y., Kakizaki, T., Sakagami, H., Saito, K., Ebihara, S., Kato, M., et al. (2009). Fluorescent labeling of both GABAergic and glycinergic neurons in vesicular GABA transporter (VGAT)-venus transgenic mouse. *Neuroscience* 164, 1031–1043. doi: 10.1016/j.neuroscience.2009.09.010
- Wang, Y., Tu, Q., Yan, W., Xiao, D., Zeng, Z., Ouyang, Y., et al. (2014). CXC195 suppresses proliferation and inflammatory response in LPS-induced human hepatocellular carcinoma cells via regulating TLR4-MyD88-TAK1-mediated NF- κ B and MAPK pathway. *Biochem. Biophys. Res. Commun.* 456, 373–379. doi: 10.1016/j.bbrc.2014.11.090
- Wang, Y., Zhao, T., Dai, P., Jiang, N., and Li, F. (2016). Employment of molecularly imprinted polymers to high-throughput screen nNOS-PSD-95 interruptions: structure and dynamics investigations on monomer-template complexation. *Chemphyschem* 17, 893–901. doi: 10.1002/cphc.201500941
- Xu, B., Zheng, H., and Patel, K. P. (2012). Enhanced activation of RVLM-projecting PVN neurons in rats with chronic heart failure. *Am. J. Physiol. Heart Circ. Physiol.* 302, H1700–H1711. doi: 10.1152/ajpheart.00722.2011
- Yamazaki, A., Yashiro, M., Mii, S., Aki, R., Hamada, Y., Arakawa, N., et al. (2016). Isoproterenol directs hair follicle-associated pluripotent (HAP) stem cells to differentiate *in vitro* to cardiac muscle cells which can be induced to form beating heart-muscle tissue sheets. *Cell Cycle* 15, 760–765. doi: 10.1080/15384101.2016.1146837
- Yao, S. Y., Natarajan, C., and Sriram, S. (2012). nNOS mediated mitochondrial injury in LPS stimulated oligodendrocytes. *Mitochondrion* 12, 336–344. doi: 10.1016/j.mito.2012.01.002
- Yu, Y., Wei, S. G., Zhang, Z. H., Weiss, R. M., and Felder, R. B. (2016). ERK1/2 MAPK signaling in hypothalamic paraventricular nucleus contributes to sympathetic excitation in rats with heart failure after myocardial infarction. *Am. J. Physiol. Heart Circ. Physiol.* 310, H732–H739. doi: 10.1152/ajpheart.00703.2015
- Yusuf, S. A. L. I. M., Theodoropoulos, S., Mathias, C. J., Dhalla, N. A. Z. I. R., Wittes, J., Mitchell, A., et al. (1987). Increased sensitivity of the denervated transplanted human heart to isoprenaline both before and after beta-adrenergic blockade. *Circulation* 75, 696–704. doi: 10.1161/01.CIR.75.4.696
- Zhang, K., Li, Y. F., and Patel, K. P. (2002). Reduced endogenous GABA-mediated inhibition in the PVN on renal nerve discharge in rats with heart failure. *Am. J. Physiol. Regul. Integr. Comp. Physiol.* 282, R1006–R1015. doi: 10.1152/ajpregu.00241.2001
- Zheng, M., Zhang, S. J., Zhu, W. Z., Ziman, B., Kobilka, B. K., and Xiao, R. P. (2000). Beta 2-adrenergic receptor-induced p38 MAPK activation is mediated by protein kinase A rather than by Gi or Gbeta gamma in adult mouse cardiomyocytes. *J. Biol. Chem.* 275, 40635–40640. doi: 10.1074/jbc.M006325200

Conflict of Interest Statement: The authors declare that the research was conducted in the absence of any commercial or financial relationships that could be construed as a potential conflict of interest.

Copyright © 2017 Ogundele, Rosa, Dharmakumar, Lee and Francis. This is an open-access article distributed under the terms of the Creative Commons Attribution License (CC BY). The use, distribution or reproduction in other forums is permitted, provided the original author(s) or licensor are credited and that the original publication in this journal is cited, in accordance with accepted academic practice. No use, distribution or reproduction is permitted which does not comply with these terms.